

High harmonic imaging of ultrafast many-body dynamics in strongly correlated systems

R. E. F. Silva,^{1,*} Igor V. Blinov,^{2,3} Alexey N. Rubtsov,^{2,4} O. Smirnova,^{1,5} and M. Ivanov^{1,6,7,†}

¹Max-Born-Institut, Max Born Strasse 2A, D-12489 Berlin, Germany

²Russian Quantum Center, Skolkovo 143025, Russia

³Moscow Institute of Physics and Technology, 9 Institutsky lane, Dolgoprudny, Moscow region 141700, Russia

⁴Department of Physics, Moscow State University, 119991 Moscow, Russia

⁵Technische Universitaet Berlin, Ernst-Ruska-Gebaeude, Hardenbergstr. 36A,10623, Berlin, Germany

⁶Blackett Laboratory, Imperial College London, South Kensington Campus, SW7 2AZ London, United Kingdom

⁷Department of Physics, Humboldt University, Newtonstrasse 15, 12489 Berlin, Germany

This Letter brings together two topics that, until now, have been the focus of intense but non-overlapping research efforts. The first concerns high harmonic generation in solids, which occurs when intense light field excites highly non-equilibrium electronic response in a semiconductor or a dielectric. The second concerns many-body dynamics in strongly correlated systems such as the Mott insulator. Here we show that high harmonic generation can be used to time-resolve ultrafast many-body dynamics associated with optically driven phase transition, with accuracy far exceeding one cycle of the driving light field. Our work paves the way for time-resolving highly non-equilibrium many body dynamics in strongly correlated systems, with few femtosecond accuracy.

PACS numbers: 78.47.J-, 71.27.+a, 42.65.Ky

High harmonic emission provides the frequency domain view of charge dynamics in quantum systems [1]. Complete characterization of the emitted harmonic light – its spectrum, polarization, and spectral phase – allows one to decode the underlying charge dynamics in atoms and molecules with resolution < 0.1 femtosecond (fs), well below a single cycle of the driving laser field, opening the new field of ultrafast high harmonic imaging [2–9].

Here we bring high harmonic imaging to many-body dynamics in strongly correlated solids, focusing on an ultrafast phase transition. We consider the breakdown of the Mott insulating state in the canonical model of a strongly correlated solid, the Fermi-Hubbard model. We show how the complex many-body charge dynamics underlying this transition are recorded by high harmonic emission, with few fs accuracy.

Combining high harmonic generation in bulk solids [10–14] with robust techniques for characterizing the emitted light [12–14] has demonstrated the capabilities of high harmonic imaging in solids. Recent results include the demonstration of the dynamical Bloch oscillations [14, 15], the reconstruction of the band structure in ZnO [16], the visualization of strong field-induced effective band structure [17], and direct visualization of the asymmetric charge flow driven by MIR fields [18]. Yet, all of these studies have been confined to systems well described by single-particle band structure, and single-particle pictures have dominated the analysis [10–12, 14, 17, 19]. The role of electron-electron correlation has been relegated to empirically introduced (and unusually short, only a few fs) relaxation times [11, 12].

Yet, electron-electron correlations go well beyond mere dephasing, generating rich physics of strongly correlated systems, such as pre-thermalization and the formation of extended Gibbs ensembles [20], superfluid to Mott insulator transition [21], to name but a few. Studies of non-equilibrium many body dynamics have lead to the concepts of the dynamical [22] and light-induced phase transitions [23–26]. In particular, the Mott insulator-to-metal transition was recently achieved experimentally in VO₂ [25, 26]. Resolving such transitions with few-femtosecond accuracy remains, however, elusive. Our results show that high harmonic imaging is ideally suited to address this challenge, offering detailed view of the underlying dynamics.

We use one-dimensional Fermi-Hubbard model with half-filling, i.e. with averaged particle density equal to one per site (see Methods for details). A particle could freely hop to an adjacent site with a rate t_0 , yielding the metallic state of the system. Hopping can be obstructed by another particle already residing on the adjacent site, via the energy U of the repulsive on-site interaction. In the strong coupling limit $U \gg t_0$, the Mott insulating ground state has short-range antiferromagnetic order [27] (the electron spins at the adjacent sites tend to be anti-parallel). The elementary charge excitations, called doublon-hole pairs [28, 29], are separated by an optical gap Δ . Deep into repulsive regime ($U \gg t_0$), Δ scales linearly with U . We focus on this regime, and consider the driving field $\omega_L \ll \Delta(U)$ in the mid-IR range, with $\omega_L = 32.9$ THz identical to that in recent experiments [12], and a modest peak amplitude $F_0 = 10$ MV/cm. The hopping rate is set to $t_0 = 0.52$ eV to mimic Sr₂CuO₃ [28], and U is varied to demonstrate the trends and the general nature of our conclusions. Details of our simulations are described in the Methods section.

To induce and resolve the Mott transition, we apply

*Electronic address: silva@mbi-berlin.de

†Electronic address: mikhail.ivanov@mbi-berlin.de

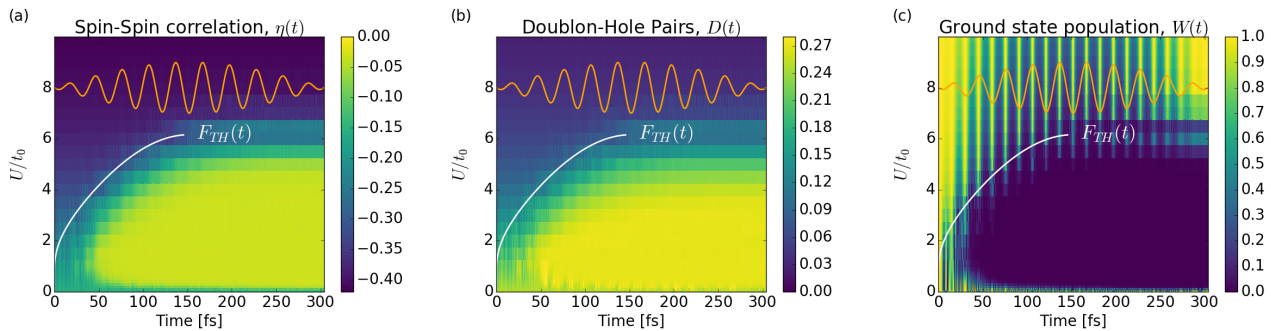


Figure 1: Time-resolved light-induced breakdown in the Mott insulator. Time-resolved spin-spin correlation (a) and the number of doublon-hole pairs (b) for a range of U/t_0 . The pulse has peak strength $F_0 = 10$ MV/cm, frequency 32.9 THz, and a 10-cycle long \sin^2 envelope. The red curve shows the time when the threshold field strength for the transition is reached. The field amplitude is insufficient for the breakdown at $U/t_0 > 6$, in agreement with F_{TH} Eq.(1). (c) Abrupt destruction of the Mott state, shown via $W(t) = |\langle \Psi_0 | \Psi(t) \rangle|^2$, occurs within a cycle for the fields exceeding the threshold.

a light pulse where the field amplitude $F_0(t)$ increases smoothly. This field can excite the doublon-hole pairs, which play the role of carrier chargers. The density of doublon-hole pairs may change during the pulse, depending on the field amplitude F_0 . As F_0 crosses the threshold F_{TH} , the density of charge carriers exceeds critical value, leading to the breakdown of the Mott insulator – the system becomes conducting. The transition is followed by the destruction of local magnetic order and a paramagnetic liquid-like state is formed [24, 28]. Smooth variation of $F_0(t)$ during the pulse allows us to track the transition as a function of time, with high harmonic response providing sub-cycle accuracy (see below). The transition is mathematically similar to strong-field ionization in atoms [28]. In particular, the parameter $\gamma = \hbar\omega_L/\xi F_0$ (where ξ is the correlation length [28]) serves as the analogue of the Keldysh adiabaticity parameter [1]. In the ‘tunnelling’ regime $\gamma \ll 1$ the threshold field is [28]

$$F_{TH} = \Delta/2e\xi \quad (1)$$

As the insulator-to-metal transition is marked by the increased density of charge carriers and the destruction of short-range magnetic order, we will characterize the state of the system via the two parameters describing the charge and spin degrees of freedom: the next-neighbor spin-spin correlation function

$$\eta = \frac{1}{L} \left\langle \sum_{j=1}^L \vec{S}_j \cdot \vec{S}_{j+1} \right\rangle \quad (2)$$

and the average number of doublon-hole pairs per site,

$$D = \frac{1}{L} \left\langle \sum_{j=1}^L c_{j,\uparrow}^\dagger c_{j,\uparrow} c_{j,\downarrow}^\dagger c_{j,\downarrow} \right\rangle \quad (3)$$

Here j labels the site, up-down arrows the spin, $L = 12$ is the number of sites, c^\dagger, c are the creation and annihilation operators.

The destruction of short range antiferromagnetic order during the transition is shown in Fig. 1 (a): within a

cycle, the spin-spin correlation function drops to nearly zero (limited by the finite size of the system). The second signature of the transition is the rise in the number of doublon-hole pairs, Fig.1 (b), which is linked to the loss of spin-spin correlation (compare Figs. 1 (a,b)). After the transition, the system reaches a photo-induced saturated state [28] and the number of pairs remains constant. The abrupt nature of the transition is shown in Fig. 1(c): for fields crossing F_{TH} the overlap probability with the initial state $W(t) = |\langle \Psi_0 | \Psi(t) \rangle|^2$ drops to zero within a laser cycle, stressing the need for sub-cycle resolution.

Naturally, the rise of optical charge excitations has to manifest in the optical response. Indeed, we find that the transition is accompanied by very characteristic high-harmonic emission, see Fig.2.

Fig. 2 (a) shows harmonic spectra for two different values of U/t_0 . In the conducting limit $U/t_0 = 0$ the emission is typical for single band tight binding model [10], demonstrating clear low-order Bloch oscillation-type harmonics associated with intra-band current (the intra-band harmonics). As expected, the harmonics are narrow and well defined. In the case of $U/t_0 \gg 1$, the spectrum is quite unusual.

First, the intra-band harmonics are strongly suppressed, in stark contrast with systems described by single-particle band structures (e.g. [10–13, 15]). Second, for the same F_0 , the spectrum becomes much broader and shifts towards orders $N \sim U/\omega_L$. This characteristic change is summarized in Fig. 2 (b), where we scan U/t_0 to demonstrate the trend. For $U/t_0 \gg 1$, the spectrum peaks near the characteristic energies of doublon-hole excitation. In the half-filled system, the first allowed charge excitations are states with single doublon-hole pairs with energies between Δ and $\Delta + 8t_0$ [28, 29]. Fig.2(b) shows that these excitations are the ones responsible for the harmonic emission. Indeed, their range, shown with red lines in Fig. 2 (b), defines the lower and upper frequencies for the harmonic emission. Thus, the emission corresponds to the one-photon transition that brings the excited system back to its initial ground state via the doublon-hole

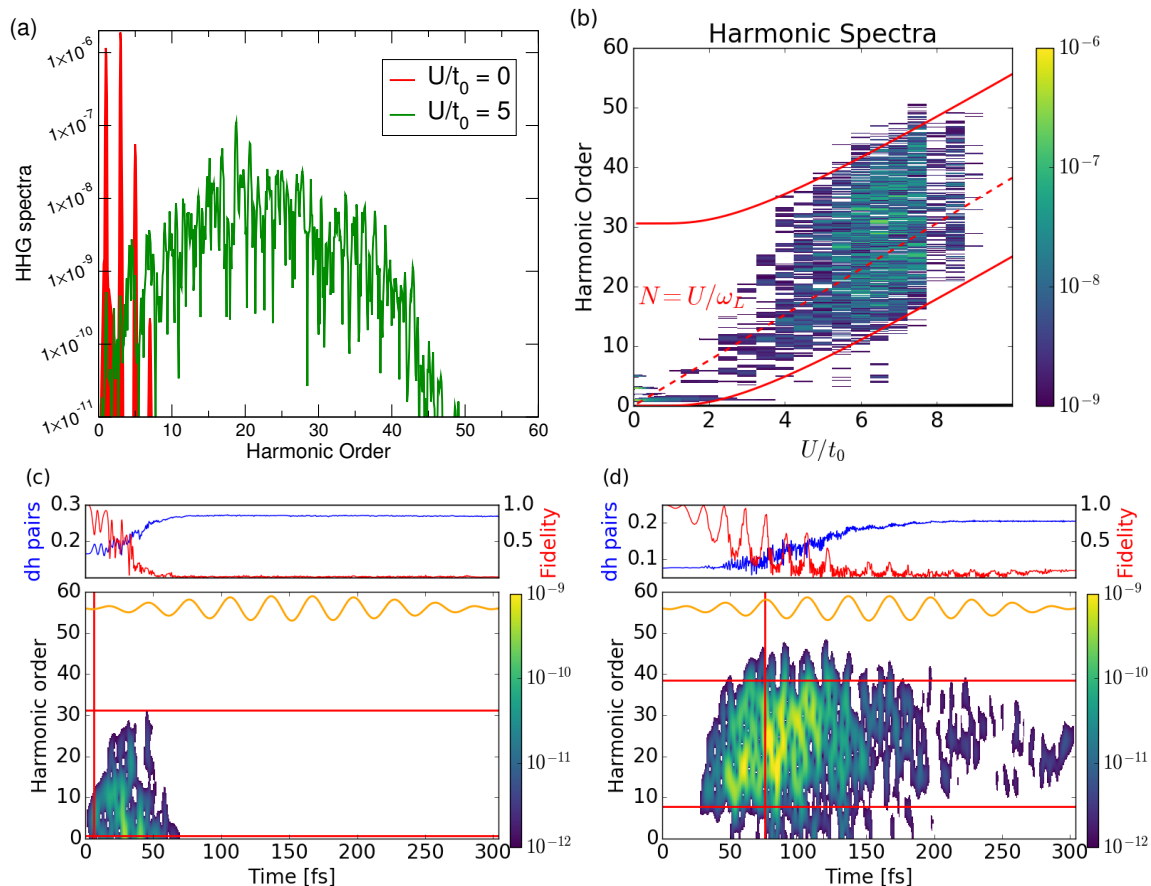


Figure 2: High harmonic spectroscopy of light-induced transition in a strongly correlated system. (a) High harmonic spectra for the conducting state, $U/t_0 = 0$ (red), and the insulating state at $U/t_0 = 5$ (green). (b) High harmonic spectrum as a function of U/t_0 . Note dramatic change in the emission spectrum in the strong coupling limit $U \gg t_0$: low harmonics are absent, the emission peaks at the characteristic energy of doublon-hole excitation $\hbar\Omega \sim U$, shown with a dashed line. Gabor profiles (c,d) of the harmonic signal for $U/t_0 = 2$ (c) and $U/t_0 = 5$ (d). The vertical red line shows when the amplitude $F_0(t)$ exceeds the threshold field F_{TH} for this value of U/t_0 . The two horizontal red lines are Δ and $\Delta + 8t_0$ for this U/t_0 . The top shows the average number of doublon-hole pairs per site (blue) and the decay of the insulating state (fidelity $\Xi(t) = |\langle\Psi_0|\Psi(t)\rangle|$, red).

recombination.

Third, the regular structure of the harmonic lines is lost in the strong coupling limit. This stands in stark contrast to weakly correlated systems, where electron-electron correlation is expected to introduce fast dephasing, the latter yielding regular, narrow harmonic lines [11]. Figs.2(c,d) clarify the physics responsible for the irregular structure of the spectrum.

Figs. 2 (c,d) show the time profile of the harmonic emission, obtained via the Gabor transform (see Methods). Note that complete time-domain reconstruction of the emitted harmonic light with $\sim 1 - 2$ fs accuracy is fully within the available experimental technology [12], for the same laser parameters as in our calculation. We see that (i) the onset of the harmonic emission is synchronized with the breakdown of the insulating Mott state and the rise in the number of doublon-hole pairs, and (ii) the fall of the emission follows the depletion of the insulating state (Fig.2(c,d)), following the

fidelity $\Xi(t) = |\langle\Psi_0|\Psi(t)\rangle|$. The Gabor profiles in Fig. 2(c,d) show that the emission takes about 50-70 fsec, i.e. only about 1-2 cycles of the driving field. The temporal restriction of the emission to a couple of cycles of the driving field explains the lack of clear peaks at odd harmonics. The complexity of the spectrum affirms the strongly aperiodic many-body dynamics, in contrast to the periodic intraband motion in the limit $U/t_0 \ll 1$ (see Fig.2(a)). The top panels in Figs. 2(c,d) confirm the conclusions drawn from Fig. 2(b): the emission relies on the coherence created between the Mott insulator ground state and the doublon-hole states. This is why it starts when the doublon-hole pairs are created and ends when the ground, Mott insulator state, is destroyed.

The lack of low-order harmonics after the phase transition leads to another important conclusion: the new many-body state created by the photo-induced transition does not support Bloch-like oscillations of doublon-hole pairs. Indeed, these would have generated strong low-

order harmonics familiar from one-electron-type excitations in a conventional conduction band. Loosely speaking, this happens because all quasi-momenta states for the doublon-hole pairs are occupied upon the transition in the tunneling regime [28].

In contrast to high harmonic emission in systems with single-particle band structure [10, 11, 14, 15], the cutoff of the harmonic signal associated with a phase transition in a strongly correlated system does not scale linearly with the electric field. In our case the harmonic emission has threshold behavior and, at $F_0 \geq F_{\text{TH}}$, covers all energies between Δ and $\Delta + 8t_0$ irrespective of the field. We also find that strong electron-electron correlations do not necessarily lead to the emergence of regular harmonic spectra with well defined lines, as expected for weakly correlated systems. Highly irregular harmonic spectra imply highly aperiodic dynamics, in line with the dramatic change in the state of the system during a phase transition.

High harmonic generation has been pioneered three decades ago [30], evolving from an unusual table-top source of bright, coherent XUV light to the technological backbone of attosecond science [1] and a unique tool for imaging ultrafast dynamics with attosecond to few-femtosecond temporal resolution [3]. Yet, throughout these decades, the analysis of high harmonic generation has been rooted in effectively single-electron pictures. Our work is the first to bring fundamental strongly correlated many-body dynamics squarely into its view.

Acknowledgments

We gratefully acknowledge fruitful discussions with Dr. Takashi Oka, Dr. Bruno Amorim, and Dr. Peter Hawkins. M. I. and R. E. F. S. acknowledge the support from the MURI programme.

Methods

We study high harmonic generation in the one-dimensional, half-filled Fermi-Hubbard model by solv-

ing the time dependent Schrödinger's equation (TDSE) numerically exactly, fully including the electron-electron correlations in the system interacting with intense light field. We use the 1D Fermi-Hubbard Hamiltonian [29]

$$\hat{H}(t) = -t_0 \sum_{\sigma,j=1}^L \left(e^{-i\Phi(t)} c_{j,\sigma}^\dagger c_{j+1,\sigma} + e^{i\Phi(t)} c_{j+1,\sigma}^\dagger c_{j,\sigma} \right) + U \sum_{j=1}^L c_{j,\uparrow}^\dagger c_{j,\uparrow} c_{j,\downarrow}^\dagger c_{j,\downarrow}. \quad (4)$$

where the laser electric field $F(t) = -dA(t)/dt$ enters through the time-dependent Peierls phase $eaF(t) = -d\Phi(t)/dt$, a is the lattice constant and $A(t)$ is the field vector potential. The hopping parameter t_0 is set to $t_0 = 0.52$ eV to mimic Sr_2CuO_3 [28], and $U > 0$ is the on-site Coulomb repulsion. In the calculations, we use the periodic boundary conditions $c_{j,\sigma} = c_{j+L,\sigma}$ with $L = N = 12$, N being the number of particles, and focus on the $S_z = 0$ subspace. Starting at $t = 0$ from the ground state of the Hamiltonian, we apply the pulse with $A(t) = A_0 f(t) \sin(\omega_L t)$ at the carrier wavelength of $9.11\mu\text{m}$ ($\omega_L = 32.9$ THz) and the peak amplitude $F_0 = \omega_L A_0 = 10$ MV/cm. All the parameters of the pulse are well within the experimental reach. The pulse has total duration of 10 optical cycles and a \sin^2 envelope, and is shown in Fig.1

To compute the harmonic emission, we first use the electric current operator, defined as [29]

$$J(t) = -ieat_0 \sum_{\sigma} \sum_{j=1}^L \left(e^{-i\Phi(t)} c_{j,\sigma}^\dagger c_{j+1,\sigma} - h.c. \right). \quad (5)$$

to compute the time-dependent current. The harmonic spectrum is calculated as the square of the Fourier transform of the dipole acceleration, $a(t) = \frac{d}{dt} J(t)$. Time-resolved emission is obtained by performing the Gabor (window Fourier) transform with the sliding window $\exp[-(t - \tau)^2/\sigma^2]$, $\sigma = (3\omega_L)^{-1}$.

-
- [1] Krausz, F. & Ivanov, M. Attosecond physics. *Reviews of Modern Physics* **81**, 163 (2009).
 - [2] Baker, S. *et al.* Probing proton dynamics in molecules on an attosecond time scale. *Science* **312**, 424–427 (2006).
 - [3] Lein, M. Molecular imaging using recolliding electrons. *Journal of Physics B: Atomic, Molecular and Optical Physics* **40**, R135 (2007).
 - [4] Smirnova, O. *et al.* High harmonic interferometry of multi-electron dynamics in molecules. *Nature* **460**, 972–977 (2009).
 - [5] Haessler, S. *et al.* Attosecond imaging of molecular electronic wavepackets. *Nature Physics* **6**, 200–206 (2010).
 - [6] Shafir, D. *et al.* Resolving the time when an electron exits a tunnelling barrier. *Nature* **485**, 343–346 (2012).
 - [7] Pedatzur, O. *et al.* Attosecond tunnelling interferometry. *Nature Physics* **11**, 815–819 (2015).
 - [8] Bruner, B. D. *et al.* Multidimensional high harmonic spectroscopy of polyatomic molecules: detecting sub-cycle laser-driven hole dynamics upon ionization in strong mid-ir laser fields. *Faraday Discussions* **194**, 369–405 (2016).
 - [9] Kraus, P. M. *et al.* Measurement and laser control of attosecond charge migration in ionized iodoacetylene. *Science* **350**, 790–795 (2015).

- [10] Ghimire, S. *et al.* Observation of high-order harmonic generation in a bulk crystal. *Nature physics* **7**, 138–141 (2011).
- [11] Vampa, G. *et al.* Theoretical analysis of high-harmonic generation in solids. *Physical review letters* **113**, 073901 (2014).
- [12] Hohenleutner, M. *et al.* Real-time observation of interfering crystal electrons in high-harmonic generation. *Nature* **523**, 572 (2015).
- [13] Langer, F. *et al.* Lightwave-driven quasiparticle collisions on a subcycle timescale. *Nature* **533**, 225–229 (2016).
- [14] Luu, T. T. *et al.* Extreme ultraviolet high-harmonic spectroscopy of solids. *Nature* **521**, 498–502 (2015).
- [15] Schubert, O. *et al.* Sub-cycle control of terahertz high-harmonic generation by dynamical bloch oscillations. *Nature Photonics* **8**, 119–123 (2014).
- [16] Vampa, G. *et al.* All-optical reconstruction of crystal band structure. *Physical review letters* **115**, 193603 (2015).
- [17] Hawkins, P. G., Ivanov, M. Y. & Yakovlev, V. S. Effect of multiple conduction bands on high-harmonic emission from dielectrics. *Physical Review A* **91**, 013405 (2015).
- [18] You, Y. S., Reis, D. A. & Ghimire, S. Anisotropic high-harmonic generation in bulk crystals. *Nature Physics* (2016).
- [19] Higuchi, T., Stockman, M. I. & Hommelhoff, P. Strong-field perspective on high-harmonic radiation from bulk solids. *Physical review letters* **113**, 213901 (2014).
- [20] Eisert, J., Friesdorf, M. & Gogolin, C. Quantum many-body systems out of equilibrium. *Nature Physics* **11**, 124–130 (2015).
- [21] Bloch, I., Dalibard, J. & Zwerger, W. Many-body physics with ultracold gases. *Reviews of modern physics* **80**, 885 (2008).
- [22] Heyl, M., Polkovnikov, A. & Kehrein, S. Dynamical quantum phase transitions in the transverse-field ising model. *Physical review letters* **110**, 135704 (2013).
- [23] Nasu, K. (ed.) *Photo-Induced Phase Transitions* (World Scientific, New Jersey, 2004).
- [24] Oka, T. & Aoki, H. Photoinduced tomonaga-luttinger-like liquid in a mott insulator. *Physical Review B* **78**, 241104 (2008).
- [25] Liu, M. *et al.* Terahertz-field-induced insulator-to-metal transition in vanadium dioxide metamaterial. *Nature* **487**, 345–348 (2012).
- [26] Mayer, B. *et al.* Tunneling breakdown of a strongly correlated insulating state in VO_2 induced by intense multiterahertz excitation. *Physical Review B* **91**, 235113 (2015).
- [27] Gebhard, F. *The Mott Metal-Insulator Transition: Models and Methods* (Springer, 1997).
- [28] Oka, T. Nonlinear doublon production in a mott insulator: Landau-dykhne method applied to an integrable model. *Physical Review B* **86**, 075148 (2012).
- [29] Essler, F. H. L., Frahm, H., Göhmann, F., Klümper, A. & Korepin, V. E. *The One-Dimensional Hubbard Model* (Cambridge University Press, 2010).
- [30] Ferray, M. *et al.* Multiple-harmonic conversion of 1064 nm radiation in rare gases. *Journal of Physics B: Atomic, Molecular and Optical Physics* **21**, L31 (1988).